Calculations on the Recoupling of Scattering Light of a Mirror Setup with a Recoil Mass into a Laser-Field

Simon Zeidler, Tomotada Akutsu, Yasuo Torii, Eiichi Hirose

Gravitational Wave Project, National Astronomical Observatory of Japan, 2-21-2 Osawa, Mitaka, Tokyo 181-8588, Japan

simon.zeidler@nao.ac.jp

Abstract: Should be texted...

OCIS codes: (000.0000) General.

References and links

Yoichi Aso. Kagra main interferometer design document. Technical report, 2014.

Eanna E. Flanagan and Kip S. Thorne. Noise due to light scattering in interferometric gravitational wave detectors. i: Handbook of formulae, and their derivations. 2011.

James E. Harvey, Sven Schröder, Narak Choi, and Angele Duparre. Total integrated scatter from surfaces with arbitrary roughness, correlation widths, and incident angles. *Optical Engineering*, (13402):11, 2012.

Andrey Krywonos. *Predicting surface scatter using a linear systems formulation of non-paraxial scalar diffraction*. PhD thesis, 2000.

Jean-Yves Vinet, Violette Brisson, Stefano Braccini, Isidore Ferrante, Laurent Pinard, Francois Bondu, and Eric Tournie. Scattered light noise in gravitational wave interferometric detectors: A statistical approach. *Physical Review D*, (10), 1997.

1. introduction

Scattering light in high-sensitive interferometers is an often discussed and well known issue and one of the main limitations of the sensitivity of such instruments (**References**). The reason for scattering is the interaction of light with surfaces having a random, isotropic structure in the dimension of the wavelength of the light (**References**). Since the randomness of surface structures relies on the nature of surface treatments (like polishing) or the randomness of environmental conditions in a microscopical scale during the development of materials, scattering in general can not be avoided.
A gravitational wave detector which is based on interferometry like KAGRA uses a lot of different optical elements (Aso, 2014). Especially mirrors are essential. Even smallest amounts of stray light that are guided by a mirror back into the main laser beam can effect the final measurement when their phase information carries a frequency distribution (Vinet et al., 1997). These frequency distributions come from surfaces others than the mirror which can re-scatter the once scattered light from the mirror. Rescattered light again can reach the mirrors and re-couple into

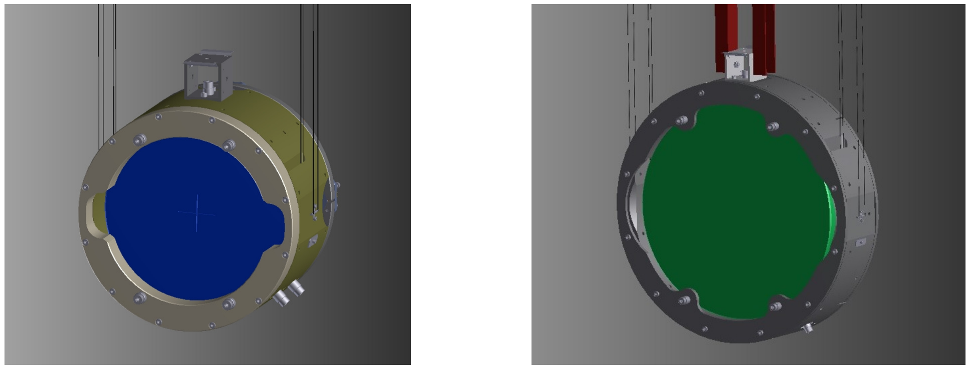

Fig. 1. Sketches of the PR/SR-mirrors (left) and the BS-mirror (right) with their respective recoil mass (shown in grey surrounding the mirror).

the main laser beam carrying now the phase information mainly from those surfaces. Guidelines for the general calculation of re- or back-scattering light and its impact on the gravitational wave strain are already existing in, for instance, Vinet et al. (1997); Flanagan and Thorne (2011) and will not be given here. However, previous papers and works concentrated only on surfaces lying relatively far away from mirrors used in gravitational wave detectors. In this paper, also surfaces close to the mirrors, and seen under wide angles from the mirrors normal vector, will be considered, in particular, the surfaces of the recoil masses which surround the mirrors in KAGRA.
Recoil masses are used to hold the mirrors and include electrical magnets corresponding to magnets attached on back-surface of the mirror to correct its respective position. In Figs. 1 and 1, the basic sketches of two main types of mirrors for KAGRA are presented: the power- and signal-recycling mirrors (PR) and the beam-splitter (BS) mirror.

2. Theoretical Approach

2.1. *Scattering on a Mirror*

The surface scattering (as well as specular reflection) on an area dA_s is in a very general way described in terms of the bidirectional-reflection-distribution-function (*BRDF*) as

$$BRDF = \frac{\partial L_s(\theta_i, \phi_i; \theta_s, \phi_s)}{\partial E_i(\theta_i, \phi_i)}. \tag{1}$$

Here, L_s is the radiance of reflected/scattered light and E_i the irradiance of the incoming light with power P_i, respectively; θ_i/ϕ_i and θ_s/ϕ_s are the incident and scattered latitude/longitude in spherical coordinates as shown in Fig. 2.1. Both radiance and irradiance depend on the specific location of the scattering event on the surface and are defined as

$$L_s = \frac{\partial P_s}{\partial A_s \cdot \cos\theta_s \cdot \partial\Omega_s}, \qquad E_i = \frac{\partial P_i}{\partial A_s}, \tag{2}$$

where P_i and P_s are the power of the incident and the scattered light, respectively. The term $\partial A_s \cdot \cos\theta_s$ is the effective radiating area an observer would see under the scattering angle θ_s. It is important to note that due to the relations

$$d\Omega_s = dA_c \cos\theta_c \cdot r^{-2} \qquad d\Omega_c = dA_s \cos\theta_s \cdot r^{-2}, \tag{3}$$

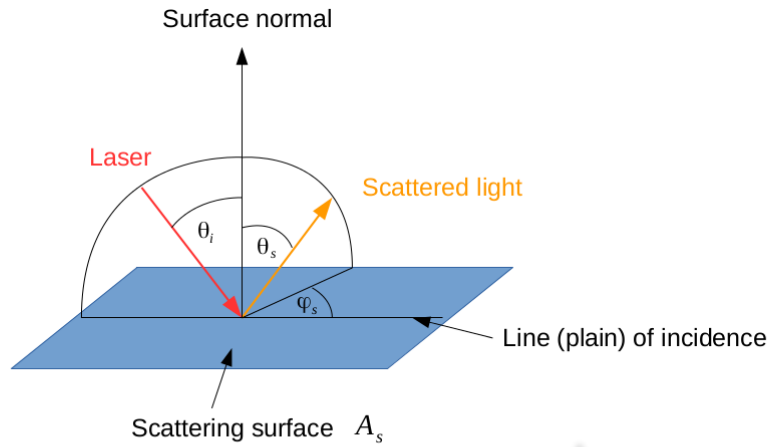

Fig. 2. Sketch of a scattering event with the principal denominations that are used in this paper. ϕ_i is set to be 0 without limiting generality.

of a source (s) and a collector (c) having a distance r to each other, L_s in Eq. (2) can be expressed also in terms of the power received by the collector[1] (Krywonos, 2000).

If now a laser hits the surface of a mirror, a small portion of the light will be scattered due to the mirrors surface properties (for high-quality mirrors, the ratio of the total integrated power of scattered light (TIS) to the power of the incident light (P_l) is usually of the order of 10^{-4} – 10^{-5}). The angular distribution of scattered light depends of course on the individual surface structure of the mirror and thus is hard to describe in general. However, it is possible to model those structures, and thus the scattering, with the aid of the surface power spectral density (PSD). The PSD can be calculated by taking the Fourier-transformation of the profile of a given surface **[some citations might be good here; or even an example of a surface map?]**. Examples for scattering models are the theories of Rayleigh-Rice, Beckmann-Kirchhoff, or (generalized) Harvey-Shack which all give an estimation of the amount of scattered light in dependence of the incident angle of a given light-field under different constraints (Harvey et al., 2012; Krywonos, 2000). In case of mirrors with smooth surfaces and small roughness, the Rayleigh-Rice theory is usually applied. However, as especially toward large scattering angle, Rayleigh-Rice (RR) shows significant difference to measurements, generalized Harvey-Shack (GHS) theory has been applied for defining the mirror scattering. GHS has been shown to be more consistent with real scattering measurements than RR (Krywonos, 2000). In a simple representation, we can write for the mirrors $BRDF$:

$$\begin{aligned} BRDF_m(\theta_i;\theta_s,\phi_s) &= \frac{16\pi^2}{\lambda^4}(\cos\theta_i{}^2+\cos\theta_s{}^2)\cdot Q\cdot PSD(f_x,f_y) \\ &= \frac{\partial L_s(\theta_i;\theta_s,\phi_s)}{\partial E_l(\theta_i)}, \end{aligned} \tag{4}$$

[1] Ω_s is the solid angle toward the detector surface and vice versa is Ω_c the solid angle from the detector toward the surface of the source.

as given in Krywonos (2000). Here, θ_s and ϕ_s are the latitude and the longitude of the scattering when light of the wavelenght λ hits the mirror under the latitude θ_i. Q is the polarization dependent reflectance of the surface for the incident angle θ_i. The two spatial frequencies f_x and f_y can be expressed in terms of θ_i, θ_s, and ϕ_s:

$$f_x = \frac{\sin\theta_s \cos\phi_s - \sin\theta_i}{\lambda} \qquad f_y = \frac{\sin\theta_s \sin\phi_s}{\lambda}. \tag{5}$$

Note: with the GHS and the RR theory one is able to describe the angular distribution of scattering but not the specular reflection itself. Also, because of the very small angular distribution of the laser light hitting the mirror (and the usually constant power), it is reasonable to write $BRDF_m = L_s/E_l$ istead of the full derivation in Eq. (4).
The *PSD* is generally two-dimensional. However, as most of the mirror surfaces are isotropic, a one-dimensional *PSD* is usually used for comparisons[2]. It is possible to reconstruct the two-dimensional form with the aid of a fitting model, called K-corellation or ABC-model (Harvey et al., 2012). I will refer to it in a kind of modified version as:

$$PSD_{1-D} = \frac{A}{(1+(Bf)^2)^{C/2}}. \tag{6}$$

Taking these parameters, the two-dimensional *PSD* can be calculated via

$$\begin{aligned} PSD_{2-D} &= K \cdot \frac{AB}{(1+(Bf)^2)^{(C+1)/2}} \\ K &= \frac{1}{2\sqrt{\pi}} \cdot \frac{\Gamma((C+1)/2)}{\Gamma(C/2)}, \end{aligned} \tag{7}$$

where we assume rotational symmetry so that $f = \sqrt{f_x^2 + f_y^2}$. The parameters A, B, and C are variable and depend on the individual surface structure. A has the dimension of PSD_{1-D} which is usually given in nm^{2}mm, while B can be interpreted as the correlation length of the surface irregularities and will be given here in mm. C has no unit and gives a measure for the slope of the *PSD*. Since the mirror surfaces that are a topic of this paper can be assumed to be isotropic **[include description of mirrors material]**, the assumption of such simple symmetric *PSD* is reasonable. However, due to the facts that neither a surface is infinitely expanded nor a measurement of its surface structure can show very small irregularitiies, a measured *PSD*, as shown in Fig. 2.1, is always limited at both small and large spatial frequencies. Thus, predictions on the *BRDF* are generally also limited to certain angular distributions around the scattering event (usually for very small and very large latitudes the *BRDF* can not be given). On the other side, even the K-correlation model sometimes fails to give the exact curve of a measured *PSD* due to additional structures or misalignments of the *PSD* curve. In such cases, it is useful to represent the measurement by a superposition of two or more K-correlation models. However, doing so, the respective *BRDF* should be calculated only within the given limits of the spatial frequency in order to avoid a non physical behavior as those structures or misalignments produce fits which are not reliable outside the mesured frequency range. In Fig. 2.1 a comparison of the measured one-dimensional *PSD* (black line) of the beam splitter of KAGRA with fits according to the ABC-model are shown. The blue line represents the sum of two independent ABC-models (red dotted and dash-dotted line, respectively) which fit the respective slopes toward higher and lower frequencies (the respective values for the parameters are given in the plot). As one fit alone would fail to give a stable representation of the *PSD*, the two fits together mimic the measurement in the given frequency range quite well.

[2] The one-dimensional *PSD* is just the average of the two-dimensional one along one of the axis.

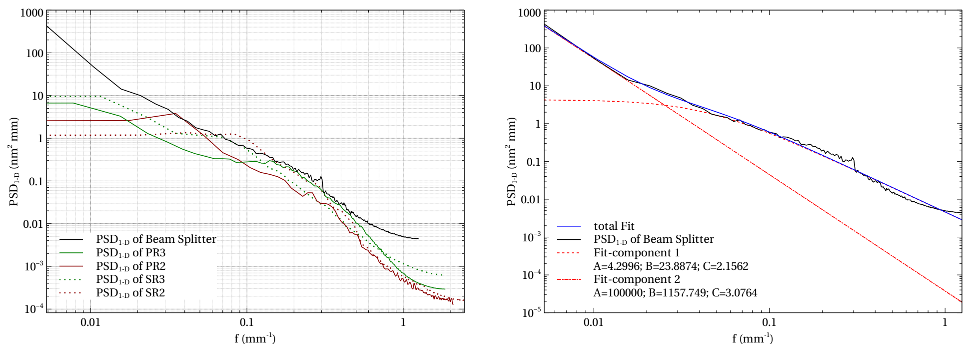

Fig. 3. Left: Comparison of the one-dimensional *PSD* of the mirrors which are investigated in this paper. Right: Fit on the measured one-dimensional *PSD* of the beam splitter of KAGRA achieved by using two independent ABC-models. Shown is the whole measured frequency range

This kind of fit was done for all mirrors for which surface-maps, and thus *PSD*s, were available, namely: PR3, PR2, SR3, SR2, and BS. For the missing PRM and SRM mirrors, we assume a similar *PSD* as for the PR2 and SR2 mirror, respectively, because of their comparable properties/requirements (see Tab. 4.1). The respective results are shown in Tab. 2.1 for the limitations of the given PSD_{1-D}. However, due to the fact that we need *BRDF* distributions of scattered light also for latitudes up to 90°, we are forced to neglect the above mentioned limitation of the fits toward higher frequencies. This has to be done in any case at some point because of the limited resolution of all surface-map measurements.

Table 1. Table of the ABC parameters of the fits on all PSD_{1-D} curves that were available at the time this paper has been written. Data for the PRM mirrors were not available.

mirror	A_1 (nm^2mm)	B_1 (mm)	C_1 (-)	A_2 (nm^2mm)	B_2 (mm)	C_2 (-)
BS	$1{\cdot}10^4$	115.77	3.08	4.3	23.89	2.16
PR3	4.6	99.46	1.91	0.29	2.03	10.17
PR2	$7{\cdot}10^{-7}$	158.71	7.49	2	17.11	2.81
SR3	$8.64{\cdot}10^{-2}$	158.83	3.59	5.98	33.79	2.35
SR2	7.69	158.79	1.88	0.9	3.17	8.79

2.2. *Scattering on Recoil Masses and Re-coupling*

We will now turn to the particular purpose of this paper which is examining the scattering on the recoil masses of the mirrors and its influence on the strain noise measured in the interferometer. Considering a laser that hits a mirror having a certain *PSD*, that particular mirror will produce scattered light during the reflection of the laser beam. If a part of this scattered power P_s is hitting the recoil mass, The again scattered light P_{ss} from the recoil mass may reach the area where the laser hits the mirror. In order to estimate that part of light, we can again apply the *BRDF* as given in Eq. (1):

$$dL_{ss} = BRDF_r \cdot dE_s = BRDF_r \cdot L_s \cos\theta_r d\Omega_r. \quad (8)$$

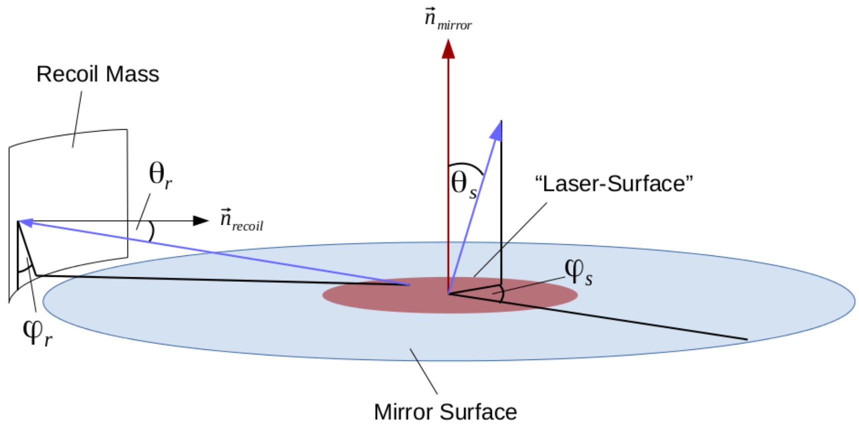

Fig. 4. Simplified sketch of the principal setup that was used for the calculations and the denomination.

Here, we used the double differential expression of the radiance and its relationship to the irradiance as given in Eqs. (2) and (3). Note that L_s is now the radiance coming from the area where the laser hits the mirror toward the recoil mass while $d\Omega_r$ is the solid angle of the recoil mass receiving L_s and θ_r is latitude of the incoming light seen from the recoil mass. Here, for simplicity, we just give the general expressions without the specific dependencies like in the equations above.

In the same way we can now formulate the power of the re-coupled light P_{sss} back into the laser:

$$L_{sss} = \frac{\partial^2 P_{sss}}{\partial A_m \cos\theta_l \partial\Omega_l} = \int_{\Omega_s} BRDF_m \cdot L_{ss} \cos\theta_s d\Omega_s. \tag{9}$$

In this expression, the index (l) marks the angles toward the waist of the laser beam while (s) is the direction from which the mirror receives the back-scattered light. This is similar to the scattering angles as used in the general expression in Eq. (4) where also $BRDF_m$ is defined. From Eqs. (2) and (3) we can rewrite Eq. (9) into

$$L_{sss} = \int_{\Omega_s} BRDF_m \cdot \frac{\partial^2 P_{ss}}{\partial A_m \partial\Omega_s} d\Omega_s. \tag{10}$$

For θ_l very close to zero (as for the PR and SR mirrors), L_{sss} can basically be calculated without the cosine-term.

2.3. *Calculation of $h_{rec}(f)$*

The frequency dependent gravitational strain $h(f)$ of the laser-light (with the wavelength $\lambda = 1.064\,\mu$m) in the cavities is what is going to be measured in a gravitational wave detector. A noisy phase shift which is carried by the stray-light from the recoil mass and is re-coupled into the main beam is disturbing this signal. This phase noise comes from motions of the recoil mass relative to the mirror, mainly caused by seismic motions, and can be described in terms of $h(f)$. Thus, we start with a somewhat general function of calculating the influence of re-coupled backscattered light on $h(f)$ after Flanagan and Thorne (2011). Defining $h_{rec}(f)$ as the influence of the stray-light of the recoil mass on $h(f)$ (light-scattering noise), it is

$$\delta h_{rec}(f)^2 = \frac{\lambda^4}{8\pi^2 L_{arm}^2 P_{mb}} \int_{\Omega_s} d\Omega_s \frac{\partial^2 P_{ss}}{\partial A_m \partial \Omega_s} \frac{\partial \rho}{\partial \Omega_l} \Phi(f)^2. \tag{11}$$

L_{arm} is the length of the arms of the interferometer (3km for KAGRA). The term $\partial\rho/\partial\Omega_l$ describes the scattering probability density of the mirror toward the laser and is basically equal to $BRDF_m \cdot \cos\theta_l$. Thus, it depends strongly on the angle of incidence of the backscattered light. Note, the reason to write δh_{rec} instead of h_{rec} is that there is still a derivation after Ω_l toward the waist of the beam which can be solved by multiplying δh_{rec} with Ω_l as Ω_l is a constant. Together with Eq. (10), we can write

$$\delta h_{rec}(f)^2 = \frac{\lambda^4}{8\pi^2 L_{arm}^2 P_{mb}} \int dL_{sss} \Phi(f)^2. \tag{12}$$

$\Phi(f)^2$ is the spectral density of the scattered light phase fluctuations at a frequency f. These fluctuations are connected to the seismic noise $\xi(f)$ of the ground that is led to the recoil mass via the respective suspension and is (in the worst case) causing a relative motion between mirror and recoil mass $\hat{\xi}(f)$. This term is determined by the specific transfer function, TF, of the suspension in horizontal and vertical direction. In frequency-space, $\hat{\xi}$ can be easily calculated by multiplying TF with $\xi(f)$ (Flanagan and Thorne, 2011) **[I should search for real published references..., e.g. Soulson]**. Thus, the spectral density of the scattered lights phase fluctuations would become $\Phi(f) = 4\pi/\lambda \cdot \hat{\xi}(f)$. However, due to the fact that only the sine of the time-dependent phase distortions of scattered light count exactly for calculating the influence on the measured gravitational wave strain **[a reference would be good]**, we have to calculate the "upconverted" noise spectrum to achieve the exact values. Basically, there are two possibilities of doing an upconversion. One is using the time dependent data of seismic noise itself and calculating the spectrum of $\sin\hat{\xi}(t)$. The other one is by using the noise spectrum and convert it by using the method of Flanagan and Thorne (2011)[3]. In Fig. 2.3 and 2.3 the spectrum of $\xi(f)$ as measured in the Kamioka mine where KAGRA is currently built is shown together with the transfered noise spectra of PR and SR mirrors and their respective upconversions.

3. Simulating Back-Scattered Light

3.1. BRDF of Recoil Mass

The above made theoretical derivation is a very general way of calculating re-coupled scattered light. The close location of the recoil mass, however, makes it very difficult (not to say impossible) to solve above equations analytically. Thus, we calculated the resulting power of the backscattered light with a numerical analysis tool for optical processes, called "LightTools".
"LightTools" uses Monte-Carlo simulation procedures to calculate probable optical paths of a huge number of virtual optical rays[4]. For interactions with surfaces, the specific properties of the surface are taken to create a probability distribution and to calculate the possible ways. While the light source creates an equal distributed set of rays, each ray carries a different power according to a given angular or spatial distribution of the emitted power.

[3] This method is relatively simple and useful but has limitations, especially when the original noise spectrum reaches values $\gtrsim 100 \cdot 4\pi/\lambda$.

[4] Depending on the complexity of the problem, simulations with approximately 2 – 20 million rays have been performed on a Dell precision T1700 PC.

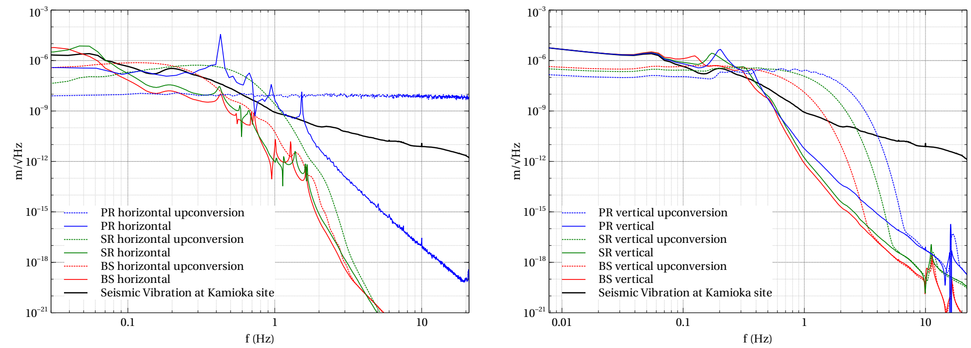

Fig. 5. Spectral density of the seismic noise of the Kamioka mine (black) and its transfered parts to the PR, SR, and BS mirrors via the respective suspensions. The horizontal part of the transfered noise is drawn in the left figure; the vertical part is drawn in the right figure. Additionally, the upconverted spectra of the transfered noise is also shown.

Depending on the mirror, the light source was set to be either the scattered light itself which comes directly from the mirror surface (as for all power-recycling and signal-recycling mirrors) or was set to simulate the laser beam before it hits the mirror (as for the beam splitter). For the first case, in order to increase the precision of the measurements, the rays were created only within the scattering angle of $\theta = 5\pi/18...\pi/2$, where a non-zero probability of hitting the recoil mass exists. In any case, the light source was set to be a circular surface with a diameter depending on the mirror that was subjected with a spatial power distribution according to a Gaussian beam with σ being the beam size as given in Table 4.1. For the PR and the SR mirrors, the angular power distribution was set according to the *BRDF* of the mirror as given in Eqs. (4) while the incident angle was set to be zero. In case of the BS (and indirectly also for the recoil mass), the properties of the surface have been changed to behave like a scatterer according to the calculations (or measurements, respectively).

The recoil masses that will be used for KAGRA are made of Titanium (roughly polished) for which the *BRDF* had to be measured in order to use the data in "LightTools" and to perform a realistic simulation. Calculated scattering values based on the surface-*PSD* could not be used in this case as the roughness of our Titanium surface is too high to perform realistic Rayleigh-Rice or Harvey-Shack calculations. A sample of such Titanium used for the measurements can be seen in Fig. 3.1). From these pictures, the rough surface can clearly be seen, especially in the measured BRDF that shows a quite noisy structure due to the surface properties. To calculate the *BRDF* we used two different scatterometers: a scatter-goniometer and a back-scatterometer[5]. Basically, for both, scattering light is produced by a $1\,\mu$m near infrared laser (a laser of the same wavelength will be used in KAGRA) hitting a sample with $10 \sim 20\,$mW. For the scatter-goniometer, the distribution of scattered light is measured by a photodiode (PD) which rotates in the plain of incident laser and specular reflection along the latitude around the scattering point on the samples surface. For the back-scatterometer, the scattering back to the incident laser beam is measured by using a beam-splitter to decouple the back-scattered light toward the PD[6]. The scattered light is measured in dependence of the angle of incidence (AOI) of the laser beam. From the measured photocurrent (I_{PC}) of the PD and its known relation to the received

[5]The particular setup of both scatterometers will be described in a later paper.

[6]The usage of a back-scatterometer is necessary as the goniometer naturally blocks the incident laser beam for latitudes where back-scattering appears.

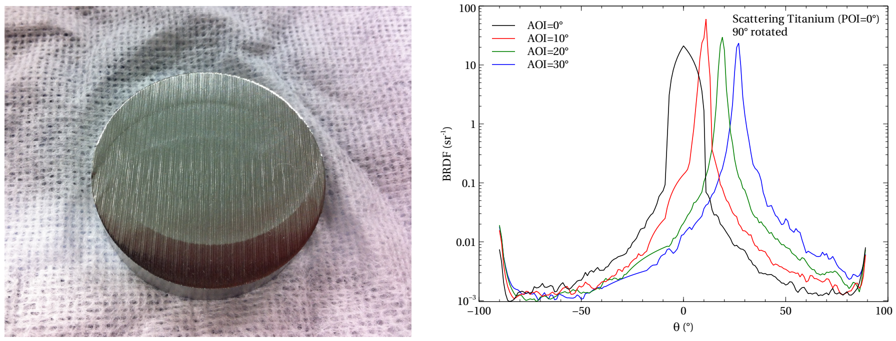

Fig. 6. Photograph of the titanium plate (left) and its scatter-profile for a 1.064 μm laser (right). The profile is a merge of scattering and back-scattering measurements.

power (n_{PD}) we can calculate the respective *BRDF* by using Eqs. (1) and (2):

$$\begin{aligned} BRDF_{bsc} &= \frac{4I_{PD} \cdot n_{PD}}{P_l \cdot \Omega_{PD} \cos(AOI)} \\ BRDF_{sc} &= \frac{I_{PD} \cdot n_{PD}}{P_l \cdot \Omega_{PD} \cos(AOI)}. \end{aligned} \tag{13}$$

The marks *bsc* and *sc* stand for back-scattering and (regular) scattering, respectively, while Ω_{PD} is the solid angle from the point of the scattering event on the sample surface toward the area of the PD ($\sim 3\,\mathrm{mm}^2$) which has a distance to the scattering point of 530 and 50 mm, respectively. The factor of 4 in the upper equation is given to the fact that for back-scattering we used a 50% beam-splitter for the measurement.

3.2. *Analyzing Simulation Results*

As a result of the simulations, a mesh of the back-scattered power P_{ss} per solid angle and surface area is created in dependence of latitude θ and longitude ϕ which are defined as discrete values. An example of such a mesh can be seen in Fig. 3.2, the result of the simulation for the PR3 mirror with the recoil mass being a Lambertian scatterer (100% reflectivity).
$\Delta P_{ss}/(\Delta A_m \Delta\Omega_s)$ shall be now abreviated as ΔI. After Eq. 11, the expected influence on the gravitational-wave strain can thus be determined to

$$\delta h_{rec}(f)^2 = \frac{2\lambda^2}{L_{arm}^2 P_{mb}} \cdot \hat{\xi}(f)^2 \cdot \sum_{i,j} \Delta I_{i,j} \cdot \Delta(\Omega_s)_{i,j} \cdot \Delta p_{i,j}. \tag{14}$$

$\Delta p_{i,j}$ represents the probability density $\Delta\rho_{i,j}/\partial\Omega_l$ of light scattered toward the waist of the laser. The sum is to be taken over all entries i and j of the corresponding mesh, related to the θ_i and ϕ_j as seen from the mirror (refers to θ_s and ϕ_s in Fig. 2.2). $\Delta(\Omega_s)$ is the corresponding solid angle mesh of the mirror. According to these equation, the intensity of the re-coupled light can be described as

$$I_{rec} = \sum_{i,j} \Delta I_{i,j} \cdot \Delta(\Omega_s)_{i,j} \cdot \Delta p_{i,j}. \tag{15}$$

4. Calculation of $h_{rec}(f)$

4.1. *Mirror Parameter*

In the upper section, it is described how the power of the stray-light re-coupling into the main beam and the strain of the interferometer is calculated in general. Now, we have to go further

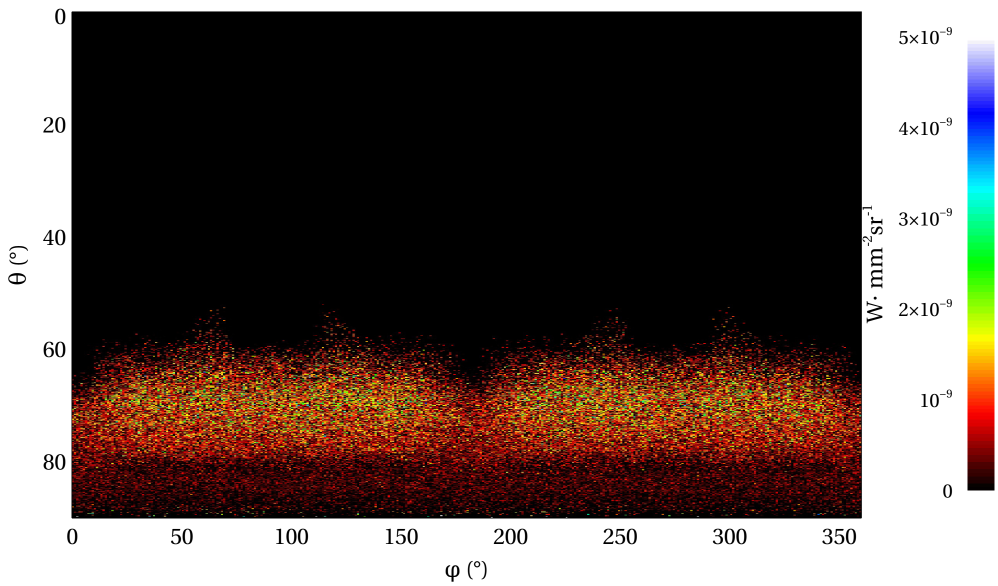

Fig. 7. Distribution of ΔI in dependence of the two angles θ and ϕ for the PR3 mirror and its recoil mass (900×360 mesh). In this simulation it was assumed that the surface of the recoil mass is a Lambertian scatterer with 100% reflectivity. The values are given in $W/(mm^2 sr)$.

and start to distinguish the power coming from different mirrors of the interferometer. The recoil masses are applied to 7 mirrors in the KAGRA interferometer. 3 for the power recycling, 3 for the signal recycling and one for the beam splitter. Since each mirror, assuming a Gaussian beam profile, provides different laser beam waist parameters (radius and distance to the mirror) in two directions, we have to deal with 12 different[7] "q"-parameters of the mirrors (q is a complex parameter that gives information on the location and the size of the waist of a Gaussian beam). From the q-parameters one is able to calculate $\Delta\Omega_l$ via

$$\begin{aligned} \Delta\Omega_l = \frac{\pi w_o^2}{R(z)^2} = \frac{\lambda q_2}{\left[q_1\left(1+\frac{q_2^2}{q_1^2}\right)\right]^2}, \\ q = q_1 + iq_2, \end{aligned} \tag{16}$$

where w_o and $R(z)$ are the beams waist and its distance to the mirror, respectively. In Tab. 4.1 the mirrors together with their respective parameter as well as the power of the main beam seen from each mirror, $\Delta\Omega_l$, and the calculated intensity of the re-coupled light according to Eq. (15) are listed.

4.2. *Results for the PR and SR Mirrors*

4.2.1. Lambertian Scatterer

As mentioned above, we distinguished two different cases. First, assuming the recoil-mass to be made of a Lambertian scatterer ("perfect" white surface) and second the case of titanium.

[7]An exception to this constrain are the PRM and SRM mirrors where only one direction is given.

Table 2. List of the mirrors, their q-parameters, the related power of the main beam P_{mb}, and the calculated results of the intensity of the stray light that is recoupled into the main beam. BS is the beam splitter, PR stands for power recycling and SR for signal recycling. The reason for the double entries of the BS, PR2, PR3, SR2, and, SR3 mirrors is they are reflective in basically two directions with non-zero incident angles (45°for BS; <1°for the other mirrors).

mirror	beam size (mm)	q_1 (m)	q_2 (m)	$\Delta\Omega_l$ (sr)	P_{mb} (W)
BS	36.1703	-1023.5	293.48	$2.5\cdot10^{-10}$	250
BS	36.0616	1020.17	293.48	$2.6\cdot10^{-10}$	250
PR3	36.6854	12.5989	0.0399461	$2.7\cdot10^{-10}$	515
PR3	36.6854	1039.26	293.48	$2.5\cdot10^{-10}$	515
PR2	4.46478	6.44215	58.1447	$2.2\cdot10^{-10}$	515
PR2	4.46478	-1.53283	0.0399461	$1.8\cdot10^{-8}$	515
PRM	4.48282	8.31934	58.1447	$3.6\cdot10^{-10}$	515
SR3	36.6846	12.5989	0.0399479	$2.7\cdot10^{-10}$	0.107
SR3	36.6846	1039.24	293.48	$2.5\cdot10^{-10}$	0.107
SR2	4.33243	7.10525	54.4941	$3.2\cdot10^{-10}$	0.107
SR2	4.33243	-1.48739	0.0399479	$1.9\cdot10^{-8}$	0.107
SRM	4.33803	7.63598	54.4941	$3.7\cdot10^{-10}$	0.107

The first case is mainly made for comparability reasons while the second case is of real interest of application. In Fig. 4.2.2 the results of the simulations for the first case are summarized and δh_{rec} is shown together with KAGRAs goal sensitivity curve (black, dotted line). For all mirrors, the results are differentiated by the horizontal and vertical vibration of their respective recoil mass. However, both kinds of vibration will influence the strain noise according to Eq. (12). Therefore, the overall noise effect can be seen as a superposition of both types of vibration. Note that the sensitivity itself is given in $\mathrm{Hz}^{-1/2}$ while $\delta h_r ec$ is given in $\mathrm{Hz}^{-1/2}\mathrm{sr}^{-1}$ as $\Delta\Omega_l$ still would have to be multiplied to get the spectral density of the gravitational wave strain noise created by the recoil mass scattering.

For all PR and SR mirrors, we find δh_{rec} to be below $10^{-24}\,\mathrm{Hz}^{-1/2}\mathrm{sr}^{-1}$ at 1 Hz and $10^{-27}\,\mathrm{Hz}^{-1/2}\mathrm{sr}^{-1}$ at 10 Hz. Compared to the sensitivity of KAGRA and taking into account that we still have to multiply $\Delta\Omega_l$ for getting the strain-noise spectral density, this is a neglible effect. Anyway it is worth to note that of all mirrors, the recoil mass of PR3 shows the biggest effect regarding the scattering noise. At 1 Hz we reach a maximum of $5.5\times10^{-25}\,\mathrm{Hz}^{-1/2}\mathrm{sr}^{-1}$ with upconverted vertical seismic noise, while, e.g., PR2 reaches only $2\times10^{-28}\,\mathrm{Hz}^{-1/2}\mathrm{sr}^{-1}$ and SR3 $5\times10^{-26}\,\mathrm{Hz}^{-1/2}\mathrm{sr}^{-1}$. This trend can be seen for all frequencies: at 10 Hz we find a maximum for PR3 at $1\times10^{-27}\,\mathrm{Hz}^{-1/2}\mathrm{sr}^{-1}$ (now from the upconverted horizontal seismic vibration), while PR2 gives $3.2\times10^{-31}\,\mathrm{Hz}^{-1/2}\mathrm{sr}^{-1}$ and SR3 only $2.6\times10^{-34}\,\mathrm{Hz}^{-1/2}\mathrm{sr}^{-1}$.

4.2.2. Titanium

The results for the case of a recoil mass made of titanium are presented in Fig. 4.2.2. Basically, the curves follow all the trends which have been discussed for the case of a lambertian scatterer. The only difference is that for titanium, all values are now reduced by a factor of ≈3.3 (the exact values for I_{rec} as given in Eq. (15) are listed in Table 4.3.1). That means, however, that also for this case, the scattering from the recoil mass won't affect the sensitivity of KAGRA.

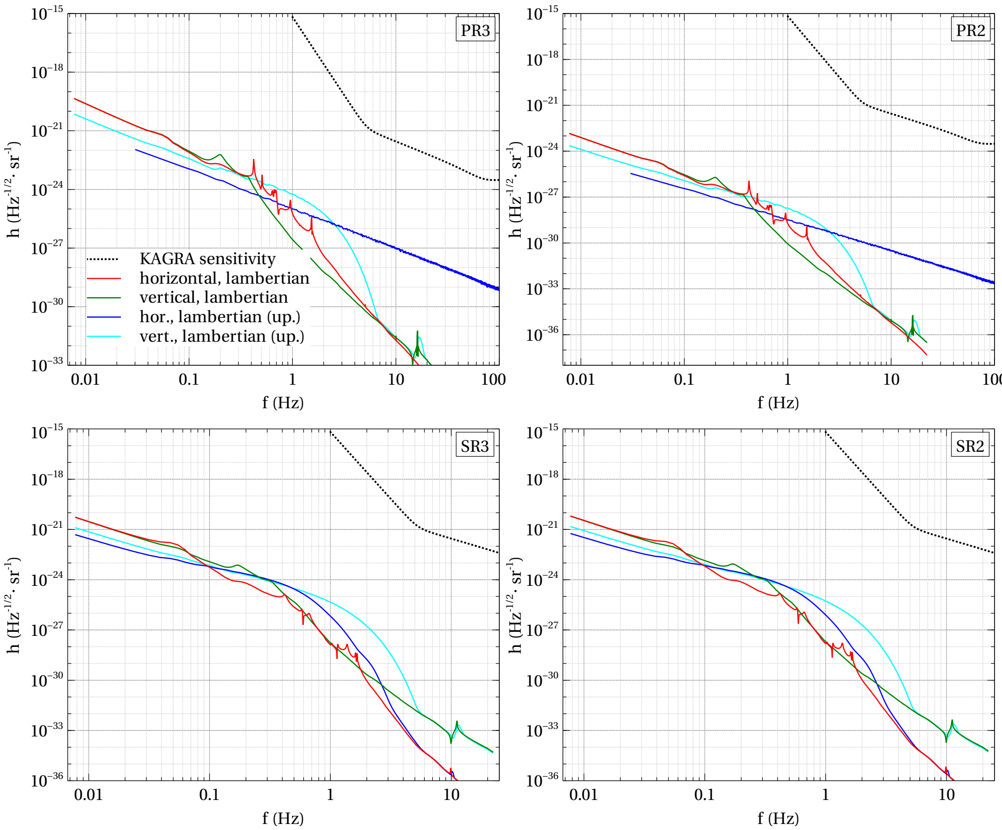

Fig. 8. Calculated strain noise (per steradiant) for the PR and SR mirrors for the theoretical case of having a recoil mass made of lambertian scatterer with 100% reflectivity in comparison with the goal sensitivity of KAGRA. Shown are the results for the vertical and horizontal movements of the mirror, together with their respective upconversion.

4.3. Results for the Beam Splitter

4.3.1. Lambertian Scatterer

In the same way as for the PR and SR mirrors, we first analyzed the case of having a recoil mass made of a Lambertian scatterer. The results of these calculations can be seen in the diagrams of Fig. 4.3.1. Alike the PR and SR mirrors, also the backside of the BS is important as the incoming beam and one beam of the arms of KAGRA hit the BS on its backside. The results for the frontside are given in the left diagram, those for the backside in the right diagram of Fig. 4.3.1. The reason why we are distinguishing these two sides is that the recoil mass on the backside of all mirrors has a different shape as it contains the EM-actuators which are needed for the mirror control (We just define the "backside" of the here discussed mirrors as the side with the actuators). Thus, the recoil mass is much bigger and we expect an actual effect on the scattering. For the alignment of the BS mirror in the interferometer, it means that the frontside is faced toward one of the 3 km arms and the SR level of KAGRA while the backside is faced to the PR level and the other arm of the interferometer (Aso, 2014). The values of $\Delta\Omega_l$ for BS (first and second entry), as given in Table 4.1, refer to the front- and to the backside, respectively.

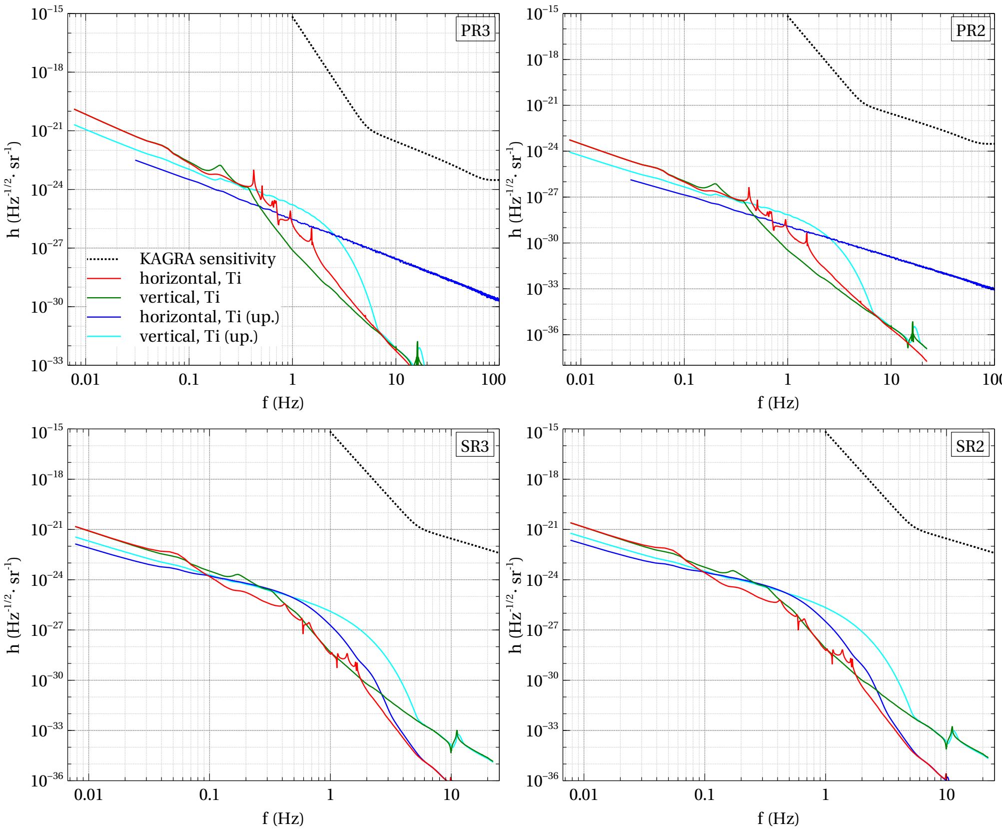

Fig. 9. Calculated strain noise (per steradiant) for the PR and SR mirrors for the case of having a recoil mass made of roughly polished Titanium in comparison with the goal sensitivity of KAGRA. Shown are the results for the vertical and horizontal movements of the mirror, together with their respective upconversion.

For all cases that are threated in this paper, the noise above 0.3 Hz is dominated by the vertical upconverted vibration while for smaller frequencies the difference between horizontal and vertical (upconverted) vibration is vanishing. In case of lambertian scatterer on the frontside, the maximum noise at 1 Hz is about $3\times10^{-25}\,\mathrm{Hz}^{-1/2}\mathrm{sr}^{-1}$. Until 10 Hz it continiously decreases down to $1.2\times10^{-32}\,\mathrm{Hz}^{-1/2}\mathrm{sr}^{-1}$. Again, the curves have to be multiplied with $\Delta\Omega_l$ as given in Table 4.1 to be comparable with the given sensitivity curve of KAGRA, which is in units $\mathrm{Hz}^{-1/2}$. On the backside, the maximum at 1 Hz is about $1.3\times10^{-24}\,\mathrm{Hz}^{-1/2}\mathrm{sr}^{-1}$, and at 10 Hz $5\times10^{-32}\,\mathrm{Hz}^{-1/2}\mathrm{sr}^{-1}$. Thus, by a factor 5 bigger than for the frontside.

Table 3. Values for I_{rec} in $\left(\frac{W}{m^2 sr^1}\right)$ as determined after Eq. (15) from the results of the simulations. The values are given for the two cases of having a Lambertian and a titanium scatterer, respectively.

I_{rec}	**BS front**	**BS back**	**PR3**	**PR2**	**SR3**	**SR2**
Lambertian	$2.94\cdot10^{-17}$	$8.13\cdot10^{-16}$	$4.04\cdot10^{-18}$	$4.16\cdot10^{-25}$	$1.19\cdot10^{-23}$	$1.63\cdot10^{-23}$
Titanium	$3.42\cdot10^{-17}$	$2.34\cdot10^{-16}$	$3.32\cdot10^{-19}$	$6.13\cdot10^{-26}$	$9.32\cdot10^{-25}$	$2.61\cdot10^{-24}$

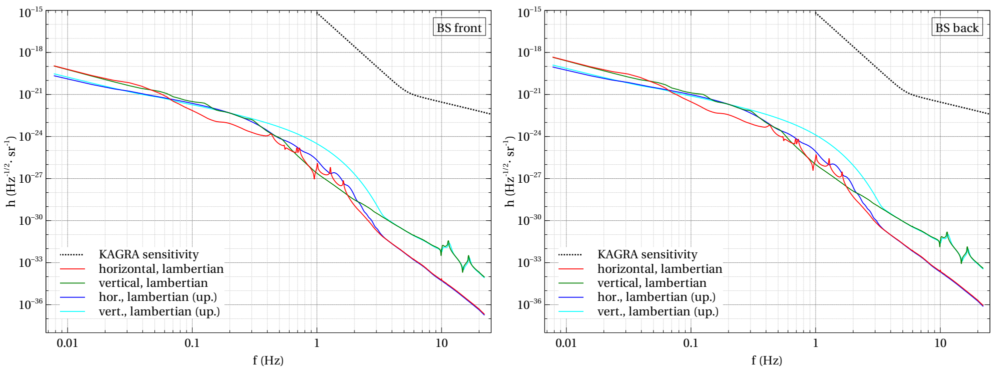

Fig. 10. The calculated spectral density of the strain noise (per steradiant) for the BS mirror having a recoil mass made of a lambertian scatterer. The data are compared with KAGRAs goal sensitivity.

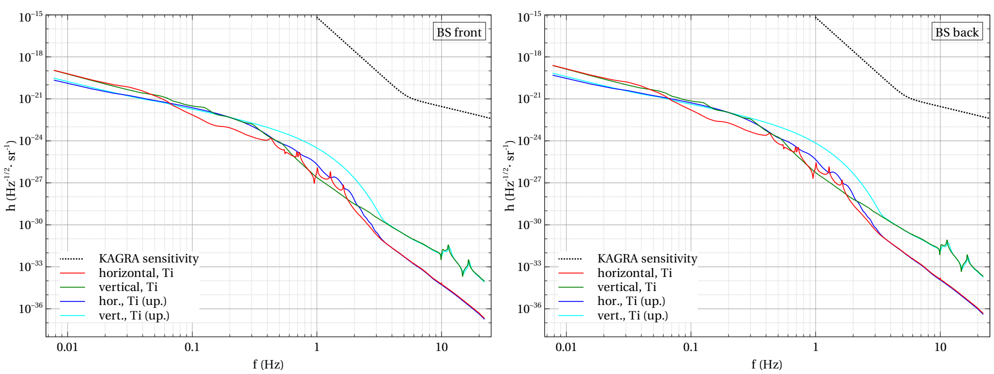

Fig. 11. The calculated spectral density of the strain noise (per steradiant) for the BS mirror having a recoil mass made of titanium. The data are compared with KAGRAs goal sensitivity.

4.3.2. Titanium

In Fig. 4.3.2, in the right diagram, the results of the calculations using the data of roughly polished titanium for the recoil mass are given. As can be seen from the pictures as well as from Table 4.1,

5. Discussion

Acknowledgements

This work was supported by MEXT, Leading-edge Research Infrastructure Program, JSPS Grant-in-Aid for Specially Promoted Research 26000005, and JSPS Core-to-Core Program, A. Advanced Research Networks.